

Dynamic loss balancing and sequential enhancement for road-safety assessment and traffic scene classification

Marin Kačan, Marko Ševrović, Siniša Šegvić

Abstract—Road-safety inspection is an indispensable instrument for reducing road-accident fatalities contributed to road infrastructure. Recent work formalizes road-safety assessment in terms of carefully selected risk factors that are also known as road-safety attributes. In current practice, these attributes are manually annotated in geo-referenced monocular video for each road segment. We propose to reduce dependency on tedious human labor by automating recognition with a two-stage neural architecture. The first stage predicts more than forty road-safety attributes by observing a local spatio-temporal context. Our design leverages an efficient convolutional pipeline, which benefits from pre-training on semantic segmentation of street scenes. The second stage enhances predictions through sequential integration across a larger temporal window. Our design leverages per-attribute instances of a lightweight bidirectional LSTM architecture. Both stages alleviate extreme class imbalance by incorporating a multi-task variant of recall-based dynamic loss weighting. We perform experiments on the iRAP-BH dataset, which involves fully labeled geo-referenced video along 2,300 km of public roads in Bosnia and Herzegovina. We also validate our approach by comparing it with the related work on two road-scene classification datasets from the literature: Honda Scenes and FM3m. Experimental evaluation confirms the value of our contributions on all three datasets.

Index Terms—Image classification, road safety, iRAP, neural networks, multi-task learning.

I. INTRODUCTION

ROAD accidents are a significant public health problem that causes more than 1.35 million deaths every year [1]. With its Global Plan for the Decade of Action for Road Safety [2], the UN has committed to halving the number of road traffic deaths and injuries by the end of this decade. The holistic "Safe System" approach [3], [4] identifies road infrastructure safety as one of the four main pillars of traffic safety [5].

Many earlier approaches to road-safety assessment estimate high-risk road sections (black spots) from historical data [6].

This work has been submitted to the IEEE for possible publication. Copyright may be transferred without notice, after which this version may no longer be accessible. Manuscript received ...; This work has been supported by project SLAIN (Saving Lives Assessing and Improving TEN-T Road Network Safety) co-financed by the Connecting Europe Facility of the European Union, Croatian Science Foundation grant IP-2020-02-5851 ADEPT, the European Regional Development Fund within the frame of the project DATACROSS (KK.01.1.1.01.0009), and NVIDIA Academic Hardware Grant Program.

M. Kačan and S. Šegvić are with University of Zagreb Faculty of Electrical Engineering and Computing (e-mail: marin.kacan, sinisa.segvic@fer.hr).

M. Ševrović is with University of Zagreb Faculty of Transport and Traffic Sciences (email: marko.sevrovic@fpz.unizg.hr)

These approaches are reactive in nature since they require accidents to occur for a section to be deemed dangerous [7], [8]. In contrast, a proactive approach to road safety is to analyze road-infrastructure features and assess in-built safety without relying on historical accident data.

While road infrastructure can be assessed via on-site surveys [9], off-line assessments are usually more practical and cost-effective [10], [11]. These assessments are currently done manually by trained operators [12]. Automating this time-consuming process is a step toward scalable road-safety assessment.

This work presents a two-stage visual recognition approach for assessment of road-infrastructure safety in monocular video. Our approach recognizes road-safety attributes directly from street-level imagery by complementing convolutional classification with sequential enhancement. We design convolutional classification as a multi-task [13] model with shared latent representation and per-attribute classification heads. We encourage high-quality latent representation by pre-training on a large street-level semantic segmentation dataset [14]. Our sequential module enhances convolutional predictions by providing access to a larger temporal context. The module consists of per-attribute LSTM models in order to account for attribute-specific temporal behavior. We address the extreme imbalance of training data by proposing a multi-task variant of dynamic loss weighting based on recall of particular classes [15]. Such practice benefits both convolutional classification and sequential enhancement.

We evaluate our approach on a novel dataset for road-safety assessment, which we denote as iRAP-BH. The dataset was acquired along 2,300km of public roads in Bosnia and Herzegovina. It covers 230,000 10-meter road segments annotated with all 52 iRAP attributes [12].

The proposed approach has no handcrafted attribute-specific rules. Hence, it could be adapted to a different road-safety programme or visual event recognition problem. We demonstrate this by testing our approach on two public road-driving classification datasets: Honda Scenes [16] and FM3m [17]. Experiments reveal that the proposed approach outperforms previous approaches on all tasks of the Honda Scenes dataset. The greatest improvements occur on the Road place task which is the most similar to iRAP attribute classification, since it contains temporal annotations and highly imbalanced classes. Our methods also perform very well on the FM3m dataset even

though the dataset is fairly well balanced as well as unsuitable for multi-frame recognition.

II. RELATED WORK

Traditional approaches to road-infrastructure assessment are based on historical accident statistics. Time, location, severity, type, and other data [18] about previous crashes can be used to identify black spots [19], create crash-risk maps [20], and design crash-prediction models [21]. These approaches can capture complex and non-trivial accident risk factors that history-agnostic approaches might overlook [8]. However, these approaches are reactive since they require accidents to occur for road sections to be assessed as unsafe [22]. Frequency-based estimation techniques also tend to produce high-variance predictions due to the sparsity of traffic accidents [23].

Proactive approaches to safe road infrastructure usually rely on periodic inspections of static features. Computer vision has been used to detect and recognize traffic signs [24], [25], road surface markings [26]–[28], fleet-management attributes [17], or semantic segmentation [29]–[32]. The recovered intermediate information can be further processed in order to detect more specific road-safety attributes [33]–[35]. For instance, Yi et al. [36] combine computer vision with active learning to detect safety features such as guardrails and utility poles. In contrast, end-to-end approaches aim to recognize road-safety attributes directly from input data [37]. Such approaches may avoid error accumulation and thus produce better latent representations.

Class imbalance refers to non-uniform class proportions within training data [38]. Data-level approaches try to rebalance the class distribution, for instance, by oversampling rare classes and undersampling frequent classes [39]. On the other hand, algorithmic-level and cost-based approaches try to adapt learning algorithms, for instance, by assigning larger loss weights to misclassified examples of underrepresented classes [40]–[43]. However, simple implementations of inverse-frequency loss-weighting improve recall at the expense of precision [15]. Tian et al. [15] address this issue by introducing dynamic assignment of class weights. During training, the class weights are dynamically updated to be inversely proportional to the current recall score of the corresponding class. This prevents classes that already achieved high recall from suffering excessive false positives. However, this approach is not directly applicable in multi-task setups.

Long short-term memory (LSTM) networks [44] have been used for video classification and action recognition [45]. Inspired by region proposal approaches [46], [47], Narayanan et al. [16] use an LSTM-based two-stream architecture to perform decoupled event proposal and temporal traffic scene classification tasks. LSTM networks have also been used for post-processing sequential predictions in speech recognition and rainfall regression [48], [49]. Recurrent networks have also been used for post-processing sequential predictions in speech recognition and rainfall regression [48], [49].

The Honda Scenes dataset considers detection of events in street video [16]. They pre-train the ResNet-50 backbone

on Places365 and leverage a pre-trained DeepLab model to ignore traffic participants. Appending semantic segmentation maps as the fourth input channel did not yield additional improvements. Their baseline approach leverages recurrent processing of frozen convolutional features and proceeds by standard softmax classification. In contrast, we use recurrent processing for enhancing existing convolutional predictions for a specific task, rather than for task-agnostic feature aggregation. Their two-stage approach generates task-agnostic event proposals as video intervals and subsequently classifies those events from spatio-temporally pooled features. Their events can be viewed as a special case of our attributes since we use multi-task instead of plain multi-class learning. A concurrent work [50] addresses recognition on Honda Scenes with a multi-task architecture that is related to our preliminary work [37]. They regularize the loss with a lower bound of mutual information between the input and features according to the Jensen-Shannon estimator [51]. None of the previous and concurrent approaches addresses rare classes with dynamic multi-task loss weighting nor do they enhance convolutional predictions with attribute-specific sequential models. Moreover, our experiments confirm the advantages of color jittering and semantic segmentation pre-training, which were presented in our preliminary study [37].

III. ROAD-SAFETY ATTRIBUTES

The internationally accepted iRAP Star Rating quantifies the overall protection that road infrastructure provides to four most common road user types in case of an accident [12]. It is calculated on 100-meter road segments using values of Crash modification factors (CMF) related to road-infrastructure features and roadside objects. There are 52 iRAP attributes that describe road infrastructure features. For a given road segment, each attribute can be in one of multiple classes. The number of classes varies across attributes. Attributes with the most classes are those that encode the speed limit (21 classes), roadside severity (17 classes), and intersection type (16 classes). On the other hand, there are 11 binary attributes. Hence, we formulate attribute recognition as separate multi-class classification problems. We had to discard four attributes that appear only in one class throughout our whole dataset. They are the following: *Shoulder rumble strips*, *Centre line rumble strips*, *Motorcycle facility*, and *Pedestrian fencing*. We also had to discard five attributes that are not suitable for our approach. These include the four speed limit attributes and *Intersecting road volume*. The latter captures the average daily number of vehicles that pass through a road segment from an intersecting road. It is not a suitable attribute for recognition in street-level video. This information is obtained from different sources, such as existing volume data or estimates based on aerial photo maps. In this way, we address 43 iRAP attributes.

A. iRAP Attribute Groups

iRAP attributes can be divided into seven groups [1].

1) *Attributes for road details and context (1 attribute)*: This group contains one attribute that describes road infrastructure: *Carriageway label*. Twelve attributes from this group encode metadata regarding data acquisition and annotation.

2) *Observed flow attributes (5 attributes)*: These attributes capture the number of motorcycles, bicycles, or pedestrians observed at a given point in time within the corresponding segment.

3) *Speed limit attributes (5 attributes)*: Four attributes in this group capture the different speed limits in a given segment. The attribute *Speed management* captures the presence of road infrastructure features such as speed bumps which reduce the operating speed.

4) *Mid-block attributes (16 attributes)*: The attributes in this group capture various features of the road itself (as opposed to its surroundings). Among those are the number and width of road lanes, the quality and adequacy of road surface and markings, the curvature, grade, and sight distance of a road section, and the presence of service roads, street lighting, and roadworks. One of the most challenging and interesting attributes in this group is the attribute *Median type*. It captures the infrastructure features that separate two opposing traffic flows. It has 15 classes that cover different types of physical separators (for divided roads) and median markings (for undivided roads).

5) *Roadside attributes (7 attributes)*: These attributes are concerned with features on both sides of the road. Thus, each attribute has a passenger-side (right) and a driver-side (left) variant. The *Roadside severity* attribute is among the most challenging attributes for automatic recognition. It has also been shown empirically to be the most time-consuming attribute for human experts to annotate manually. *Roadside severity* captures the object with the highest risk (or severity) on each of the roadsides. The relative severity of a given object on the roadside is determined by the object type and its distance from the road. Ground truth value for this attribute is assigned according to a priority table which lists each possible combination of object type and distance and is sorted according to decreasing severity.

6) *Intersection (5 attributes)*: These attributes capture various intersection features. The main attribute is *Intersection type*. It has 17 classes which cover various combinations of the number of intersecting legs, the presence of signalization, and the presence of protected turn lanes, along with other specific types of intersections (roundabouts, railway crossings, merge lanes, etc.).

7) *Vulnerable road user facilities and land use*: These attributes capture the characteristics of the area surrounding the segment (Area type, Land use, School zone), as well as the presence of facilities for cyclists and pedestrians, such as crossings and sidewalks.

B. Attribute analysis

We provide a conceptual and empirical analysis of various aspects of the iRAP attribute set in our dataset.

1) *Class imbalance*: Many attributes in our dataset suffer from significant class imbalance. We consider an attribute imbalanced when there is a significant disproportion among the number of examples belonging to different attribute classes. Class imbalance can hamper the performance of accuracy-oriented classifiers, resulting in the minority classes being

ignored. We thoroughly study and address this issue through improved loss functions, training procedures, and macro-F1 evaluation.

2) *Non-orthogonal design*: Some iRAP attributes capture multiple features that seem orthogonal to each other, resulting in classes that are (nearly) cartesian products of different values of those features. For example, the attribute *Skid resistance* is supposed to capture the skidding resistance and the texture depth of the road surface. It covers two dimensions: whether the surface grip is low (“poor”), medium, or adequate; and whether the road is sealed or unsealed. This results in the attribute having the following 5 classes: *Unsealed - poor*, *Unsealed - adequate*, *Sealed - poor*, *Sealed - medium*, *Sealed - adequate*. The attribute might have been divided into two attributes: *Sealed road* (true/false) and *Surface grip* (poor/medium/adequate). An orthogonal formulation of these concepts would mitigate the issue of class imbalance since there would be fewer classes with more examples.

3) *Fine-grained and visually similar classes*: Some attributes have very fine-grained classes that can be visually very similar. For instance, the attribute *Roadside severity* contains classes that cover different types of safety barriers (metal, concrete, wire, motorcycle friendly) and a separate class for semi-rigid structures, such as various fences. These classes are well defined, but the many options make it easy to miss the correct answer and exacerbate the issue of class imbalance by spreading the already infrequent examples over many classes.

In general, it might be advantageous to design attribute sets with fewer and more general classes. Such a decision would trade off precision and specificity of the attribute in order to decrease class imbalance.

C. Temporal analysis

The videos in our dataset cover long road sections. A road section is composed of a sequence of successive 10-meter segments. We identify several distinct patterns of temporal attribute behavior along the sequence. Some attributes have a default, “negative”, class. These attributes are usually concerned with capturing countable occurrences of various infrastructure elements, such as intersections or pedestrian crossings. The default class in these attributes is *None*, and the “positive” classes are all different types of such elements that can occur (e.g., *3-leg intersection*). Any occurrence of a positive class should be detected only in the segment closest to the occurrence. All other neighboring segments should be in the negative class. We call such attributes “single-peak” attributes.

Let us consider a segment that contains an occurrence of a positive class (a peak) and a few neighboring segments which appear immediately before it. The visual features that a model might use to discriminate among classes of such an attribute might also be present in those neighboring segments. For example, an intersection gradually becomes more visible in the segments leading up to the peak segment. A model that predicts an intersection in the neighboring segments is not entirely wrong, and it might be hard for it to discern which exact segment is the peak one.

Another example of peculiar temporal behavior is the attribute *Street lighting*, which is treated as a single-peak attribute when a single light post appears in isolation. On the other hand, for a sequence of light posts, street lighting should be recognized in all segments from the first to the last light post. This includes the segments between light posts. Since the light posts in such sequences can be up to ten segments apart, it may be difficult for a vision-based model to differentiate between single occurrences and sequences of street lights.

There is another subset of attributes that is opposite in nature to single-peak attributes. We call these attributes "smooth" since their classes rarely change and generally do not oscillate. They describe larger areas, environments, zones, or infrastructure features likely to remain unchanged in consecutive segments. Examples of such attributes include *Area type*, *Road delineation*, *Carriageway label*, etc.

We analyzed the temporal behavior of attributes by considering class co-occurrences among consecutive segments. For a given attribute A and a given pair of consecutive segments t and $(t+1)$, the pair of corresponding classes $(c_{A,t}, c_{A,t+1})$ constitutes a single co-occurrence. For an attribute with n classes, we can construct an $n \times n$ co-occurrence matrix where the element (i, j) corresponds to the number of occurrences where $c_{A,t} = i$ and $c_{A,t+1} = j$. We build two such matrices for each attribute - one using the ground truth labels and the other using predictions produced by our convolutional model.

For single-peak attributes, the only ground truth transitions that can occur are those from the default class to a positive class and back. Thus, their ground truth matrices will have non-zero elements only on the row and column corresponding to the default class. For smooth attributes, most consecutive segments belong to the same class. Thus, we expect the diagonal elements of their ground truth matrices to be significantly larger than non-diagonal elements.

We noticed consistent discrepancies between the ground truth and prediction matrices for these two groups of attributes. In prediction matrices, single-peak attributes had non-zero values outside the row and column of the default class, mainly concentrated on the diagonal. These are cases where the model assigns the same positive class to two consecutive segments which are visually very similar (e.g., two segments inside an intersection). This is a reasonable error, but it shows that the visual recognition model has not learned the single-peak annotation convention. On the other hand, for smooth attributes, significantly larger values of off-diagonal elements were observed in prediction matrices compared to ground truth matrices. This suggests there are spurious class transitions in our model's predictions for consecutive segments and that the model has not learned the general smoothness of the attribute.

Prompted by this analysis, we propose incorporating per-attribute sequential enhancement that could learn temporal behavior patterns and enhance convolutional predictions without requiring costly backpropagation through hundreds of video frames.

IV. MODEL

Our approach performs attribute recognition in two stages: convolutional classification and sequential enhancement.

A. Convolutional classification

Figure 1 illustrates our convolutional model for visual recognition in street-level imagery. The model consists of a shared front-end and attribute-specific back-ends. The front-end is based on ResNet-18 backbone which we pre-train for semantic segmentation on the Vistas dataset [14]. The resulting features are subjected to spatial pyramid pooling (SPP) with grid dimensions (6, 3, 2, 1) [52]. The SPP module captures information at different scales and produces an image-wide fixed-size vector.

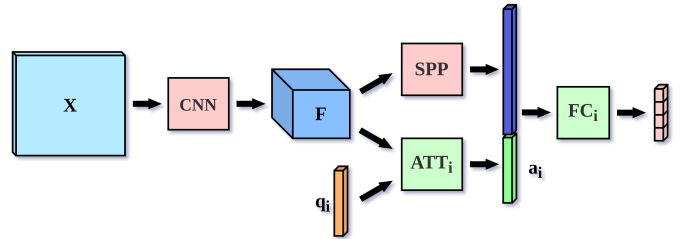


Fig. 1. The shared front-end (red) of our single-frame recognition model produces convolutional features (\mathbf{F}) that are pooled by the image-wide spatial pyramid pooling module (SPP). The attribute-specific back-ends (green) concatenate per-attribute attention pools (ATT_i) with the shared image-wide pool SPP and deliver predictions through classification heads FC_i . In the multi-frame case, the classification heads receive concatenations of single-image representations ($SPP(\mathbf{F}_t), ATT_i(\mathbf{F}_t)$), where $t \in \{1..T\}$.

Each of the 43 attribute-specific back-ends start with attention pooling ATT_i [37] with respect to attribute-specific learned query q_i . The resulting vector is concatenated with the shared SPP output and fed to the corresponding prediction head $P(A_i|x)$.

This architecture is easily extended for multi-frame input. In this case, the shared front-end is applied to each frame independently and the resulting representations are concatenated into a single vector. Per-attribute back-ends remain the same as in the single-frame case. Note that the number of input frames can not be arbitrarily large in order to avoid memory exhaustion during training. All our multi-frame models produce predictions for frame T by observing middle frames of segments $T, (T-1)$, and $(T-4)$.

Each per-attribute prediction head is subject to the corresponding cross-entropy cross. Following the multi-task learning paradigm [13], the total loss is the mean of all per-attribute losses.

B. Dynamic loss weighting for multi-task learning

We wish to alleviate undesired effects of imbalanced data by increasing the influence of rare classes to the training objective. We denote our training set with $\{x_n, y_n\}$, where $x_n \in R^d, y_n \in \{1, \dots, C\}, n \in \{1, \dots, N\}$. We let $P_n^c = P(Y = c|x_n)$ be the predicted posterior probability of class c for a given input x_n . The standard cross-entropy can be interpreted as negative logarithm of the geometric mean posterior of the correct class over all examples [15]:

$$\begin{aligned} \text{CE} &= -\frac{1}{N} \sum_{n=1}^N \ln P_n^{y_n} = -\frac{1}{N} \ln \left(\prod_{n=1}^N P_n^{y_n} \right) \\ &= -\ln \left(\prod_{n=1}^N P_n^{y_n} \right)^{\frac{1}{N}} = -\ln \bar{P} \end{aligned} \quad (1)$$

The symbol $\bar{P} = \left(\prod_{n=1}^N P_n^{y_n} \right)^{1/N}$ denotes the geometric mean posterior over all examples. This equation can also be written as a weighted sum of per-class means \bar{P}^c :

$$\begin{aligned} \text{CE} &= -\frac{1}{N} \sum_{c=1}^C \sum_{n:y_n=c} \ln P_n^c = -\sum_{c=1}^C \frac{1}{N} \ln \left(\prod_{n:y_n=c} P_n^c \right) \\ &= -\sum_{c=1}^C \frac{N_c}{N} \ln \left(\prod_{n:y_n=c} P_n^c \right)^{\frac{1}{N_c}} = -\sum_{c=1}^C \frac{N_c}{N} \ln \bar{P}^c \end{aligned} \quad (2)$$

The range $\{n : y_n = c\}$ denotes examples that belong to class c . The symbol $\bar{P}^c = \left(\prod_{n:y_n=c} P_n^{y_n} \right)^{1/N_c}$ denotes the geometric mean posterior of the correct class in samples that belong to class c . The equation shows that standard cross-entropy maximizes the weighted arithmetic mean of per-class geometric mean posteriors, with the weights being the relative class frequencies N_c/N .

If we want each class to have the same contribution to the loss, we can assign a weight to each class that is the inverse of its relative frequency: $w_c = N/N_c$. This yields the inverse-frequency-weighted cross-entropy loss [41], [42]:

$$\begin{aligned} \text{CE}^{\text{IFW}} &= -\frac{1}{N} \sum_{n=1}^N w_{y_n} \ln P_n^{y_n} = -\frac{1}{N} \sum_{c=1}^C w_c \sum_{n:y_n=c} \ln P_n^{y_n} \\ &= -\sum_{c=1}^C \frac{1}{N} w_c \frac{N_c}{N} \ln \bar{P}^c = -\sum_{c=1}^C \frac{1}{N} \ln \bar{P}^c \end{aligned} \quad (3)$$

The standard cross-entropy does not take into account the distribution of the posterior over incorrect classes. In that sense, cross-entropy can be viewed as measuring how much of a false negative a certain prediction is while ignoring false positives. Thus, assigning a large weight to a particular class might also increase the incidence of false positives for that class. This analysis has been confirmed empirically [15]: increasing the weight of a given class indeed decreases its precision.

These observations suggest that placing a large weight on a rare class that already achieves high recall might decrease precision with little gain in recall. This can be prevented by adapting the loss weights with respect to the model performance in terms of per-class recall [15]. Let $R_{c,t}$ denote the validation recall of class c after epoch $t-1$. Then, recall-based class weights $w_{c,t}^R$ can be expressed as [15]:

$$w_{c,t}^R = \frac{N}{N_c} (1 - R_{c,t}) \quad (4)$$

When recall is close to zero, the weight (4) approaches the inverse relative frequency. As the recall of a class increases, its weight diminishes.

We note that batches with examples from extremely rare classes will have a much larger loss magnitude than batches with no such examples. Hence, learning with small batches and large class imbalances may lead to drastic changes in loss magnitude across training iterations.

In multi-task learning, the total loss is calculated as the arithmetic mean over all individual tasks. Thus, a task with examples from rare classes may suffocate other tasks due to a larger loss. If we have many tasks that suffer from class imbalance, it is not unlikely that for any given batch, there will be one task that impedes the progress of other tasks. This renders the network unable to learn any of the tasks, since they all intermittently hamper each other. We address this problem by favoring a stable loss magnitude of individual tasks. We can achieve this by normalizing the loss with the sum of the weights of individual examples. If we reuse the weights w_{ct}^R from equation 4, then the loss for any individual task can be expressed as follows:

$$\text{CE}_{\text{MT}}^R = \frac{-\sum_{n=1}^N w_{y_n,t}^R \ln P_n^{y_n}}{\sum_{n=1}^N w_{y_n,t}^R}. \quad (5)$$

C. Sequential enhancement

Figure 2 shows that our sequential module enhances convolutional predictions by aggregating evidence within a large temporal window. The convolutional head for attribute a delivers convolutional logits \mathbf{s}_i^a and the index of the winning class $c_i^a = \arg \max \mathbf{s}_i^a$. We form temporal inputs as sequences of $T = 21$ vectors for all consecutive segments from $(t-10)$ to $(t+10)$. Each vector in the sequence is a concatenation of the logit vector \mathbf{s}_i^a and the learned embedding of the winning class $E_{c_i^a}$. The embedding $E_{c_i^a}$ has $\max(4, C)$ dimensions where C denotes the number of classes.

Instead of hand-crafted post-processing rules, we propose to classify prediction sequences by a bidirectional long short-term memory model (Bi-LSTM) [53]. While the first stage of our approach predicted all attributes in a single forward pass, sequential post-processing involves one Bi-LSTM for each attribute. Thus, these models can learn attribute-specific temporal behavior patterns. Each layer processes the sequence in two directions using two separate unidirectional LSTM networks. The hidden state dimension of both networks in all layers is 128. The last hidden state of a Bi-LSTM layer is the concatenation of the last hidden states produced by the two unidirectional LSTM networks. The final representation of the input sequence is created by concatenating the last hidden state vectors of all layers, together with the hidden state of the middle element of the last layer. This results in a vector of size 1280, which is then fed to a fully-connected softmax classifier. The output is the predicted posterior probability distribution over classes $P(A_i = c_{i,j} | x_{t-T:t+T})$. The network is trained using dynamically weighted cross-entropy as presented in IV-B.

V. DATASETS

A. iRAP-BH

For the purposes of off-line road-safety assessment, a novel corpus of georeferenced video was acquired along 194 public

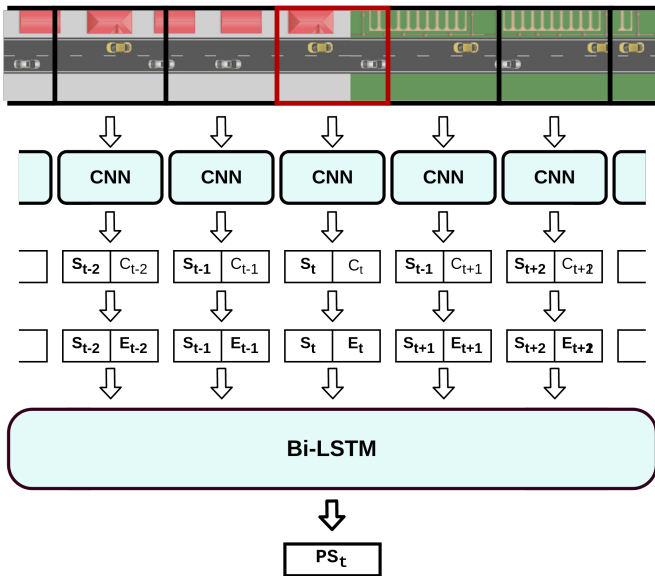


Fig. 2. The sequential enhancement module corrects CNN predictions by per-attribute Bi-LSTM models. Each Bi-LSTM model outputs corrected logits PS_t in segment t by observing $T = 21$ vectors that correspond to segments from $(t-10)$ to $(t+10)$. Each of these vectors is a concatenation of the logits S_i and the learned embedding E_i of the predicted class C_i where $i \in \{t - T : t + T\}$.

road sections (2300 km total) in Bosnia and Herzegovina. All videos were recorded in 2704x2028 RGB format at 25 frames per second. An average road section comprises 1175 segments, while an average segment spans 18 frames.

The corpus was annotated with all iRAP road-safety attributes by trained human annotators. Even though the iRAP Star Rating Score requires a 100-meter granularity of road segments, the corpus was annotated over 10-meter segments in order to provide better supervision for learning algorithms. We split the segments into 214,073 for training, 5,813 for validation, and 6,563 for testing. The training, validation, and test splits were created such that any two segments that belong to the same road section also belong to the same split. This enables us to train sequential and multi-frame models without data leakage. We represent each road segment with its middle frame resized to 384x288. This results in a multi-task multi-class video classification dataset with 226,449 images.

B. Honda Scenes

The Honda Scenes dataset contains 100 videos that are split into 80 videos for training and 20 videos for evaluation. Each frame of each video is annotated for the following four traffic scene classification tasks: *Road place*, *Road environment*, *Road surface*, *Weather*.

Images for the road place and road environment tasks have been obtained by sampling all videos at 3Hz. This results in 760,000 sequential frames for training and 160,000 frames for evaluation. We evaluate our methods by treating consecutive frames as consecutive road segments.

Images for the road surface and weather tasks have been sampled from Honda Scenes videos and complemented with a subset of frames from the BDD100k classification dataset.

The road surface dataset consists of 10,139 images, with 2,676 images from the Honda dataset and the rest from the BDD100k dataset. The training and evaluation splits contain 9,150 and 898 images, respectively. The weather dataset is a subset of the BDD100k dataset, containing 13,036 images. The training and evaluation splits contain 11,781 and 1,255 images, respectively. The following paragraphs briefly describe the four tasks.

1) *Road place*: This is the only task that considers multiple multi-class classification subtasks. Each of those subtasks has fine-grained temporal annotations with labels such as Approaching (A), Entering (E), and Passing (P) that depend on the relative position of the car to the place of interest in a given frame.

The subtasks are the following: *Construction zone*, *Intersection (3 way)*, *Intersection (4 way)*, *Intersection (5 way & more)*, *Overhead bridge*, *Rail crossing*, *Merge - Gore On Left*, *Merge - Gore On Right*, *Branch - Gore On Left*, *Branch - Gore On Right*, *Background*.

This task is the most similar to iRAP attribute classification because the subtasks consist of road infrastructure elements annotated temporally through sequential frames.

2) *Road environment*: This task involves recognition of the following classes: *Local*, *Highway*, *Ramp*, *Urban*. The task does not involve temporal labels like Road place, but it consists entirely of frames from the Honda Scenes dataset. That means we can still use our multi-frame and sequential models.

3) *Surface*: In this task, each image is annotated with one of three road surface classes: *Wet*, *Dry*, and *Snow*. Since we cannot use our multi-frame or sequential models with this task, we use the single-frame version of our model. The classes in the task are fairly balanced, so weighted losses do not improve performance.

4) *Weather*: This task involves image classification into four classes: *Clear*, *Overcast*, *Rainy*, and *Snowy*. Similarly to the Road surface task, we can only employ our single-frame model for this task.

C. FM3m

The third iteration of the Fleet Management Dataset (FM3) [17] consists of 11,448 images of traffic scenes from Croatian roads. The main subset of the dataset (FM3m) consists of 6,413 images. The training, validation and test splits contain 1,607, 1,600, and 3,206 images, respectively. Each image is labeled with one binary label (true/false) for each classification task. There are 8 classification tasks: *highway*, *road*, *tunnel*, *exit*, *settlement*, *overpass*, *booth*, *traffic*.

A large majority of images were obtained by sampling from driving videos and thus capture sequences of consecutive road segments. The frames were assigned to training, validation, and test splits in a uniform random fashion. This means that, in general, consecutive frames were assigned to different splits. This prevents us from applying models that take multiple segments as input, so we only use single-frame models in these experiments, just as in the Road surface and Weather tasks of the Honda Scenes dataset.

VI. EXPERIMENTS

We evaluate visual recognition of road-safety attributes with different variants of our approach on the iRAP-BH dataset. We compare our approach with related work on two related datasets: Honda Scenes and FM3m. Though not annotated for iRAP attributes, these two datasets were collected and labeled for classification of road and traffic-related classes, some of which are quite similar to certain iRAP attributes.

A. Evaluation metrics

We evaluate our approaches on iRAP-BH and Honda Scenes according to the mean macro-averaged F1 score [54], [55]. This is a suitable metric due to the multi-task multi-class setup, and class imbalance. The creators of Honda Scenes also use macro-F1 in their experiments.

We evaluate FM3m performance according to the mean average precision (mAP) across all tasks. This metric is suitable since all tasks are binary classification tasks. The same metric was used in the original paper [17].

B. iRAP-BH

We configure the visual recognition model according to our preliminary validation experiments [37]. Thus, we use a Vistas pre-trained ResNet-18 backbone, take three frames on input, and use color jittering as the only data augmentation procedure. For each road segment t , we consider three mid-segment image frames for segments t , $t-1$, and $t-4$. The input image resolution is 384x288. Both stages are trained using the Adam optimizer. For convolutional classification, the learning rate is set to $1e-5$, weight decay is $1e-3$ and batch size is 12. Sequential enhancement is trained with a learning rate of $5e-4$, weight decay of $1e-4$ and a batch size of 32.

We explore the impact of sequential post-processing and loss weighting on the overall performance. Table I shows that inverse-frequency weighting improves the total performance by nearly 1.5 percentage points (pp). Dynamic re-weighting delivers an additional increase of 1.3 pp. Finally, sequential post-processing further increases the performance by about 5.1 pp.

TABLE I
IMPACT OF DYNAMIC LOSS WEIGHTING AND SEQUENTIAL ENHANCEMENT ON OVERALL MACRO-F1 PERFORMANCE ON iRAP-BH.

Model	Macro-F1
Convolutional model, CE loss	54.96
Convolutional model, InvCE loss	56.43
Convolutional model, RecallCE loss	57.77
LSTM sequential model, CE loss	59.68
LSTM sequential model, RecallCE loss	62.86

The attributes which get the largest relative improvement from loss weighting are *Pedestrian crossing - inspected road*, *Median Type*, *Pedestrian observed flow along the road passenger-side*, *Roadside severity - driver-side object*, and *Bicycle facility*. Relative improvements compared to standard cross-entropy for those attributes range from 19% to 26.5%. All of these attributes suffer from class imbalance.

Single-peak attributes which benefit most from sequential post-processing are *Speed management / traffic calming* and *Intersection type*, with relative improvements of 44.7% and 22.3%, respectively. Smooth attributes with the largest relative improvements are *Bicycle facility*, *Number of lanes*, and *Skid resistance / grip*. Figure 3 shows examples of successful label corrections for several attributes. In the case of *Intersection type*, the sequential model corrected the labels to accommodate the single-peak annotation convention. For smooth attributes *Bicycle facility* and *Number of lanes*, the sequential model used the information from a larger context window to fix the spurious class transition made by the vision model. The last example is *Street lighting*, which should be annotated continuously through all segments between two nearby lighting poles. In the particular example, the upcoming lighting poles are obscured by the road curvature and overgrown roadside bushes. Because of this, the vision model does not label the in-between segments as containing street lighting. The sequential model leverages a larger context window to correct these mistakes. Table II shows how our best model performs on all attributes.

C. Honda Scenes

We compare our method with two sequential approaches presented by the dataset authors [16]. We shall denote their baseline as Honda BiLSTM, and their two-stage approach as Honda Event. We also compare our method with another multi-task approach [50] that we denote as Context MTL.

1) *Road place*: Table III shows the overall results when averaged over all classes of all subtasks. Table IV compares our models with previous and concurrent approaches. Our multi-frame convolutional model trained with standard cross-entropy loss achieves better performance than previous approaches. Loss weighting increases performance by 2.89 pp. This is because multiple subtasks suffer from class imbalance [16], most notably: *Intersection (5-way or more)*, *Railway*, *Left Merge*, and *Left Branch*. These subtasks improve the most after the addition of loss weighting, with relative improvements between 15% and 50%. Our combined approach further improves performance by 3.93 pp.

2) *Road environment*: Table V shows that our multi-frame convolutional model outperforms previous approaches on all classes except class *Local*. The largest improvement occurs for the most challenging class, *Ramp*. That is also the least frequent class in the dataset and one which benefits the most from loss weighting. Our combined model further improves total performance by an additional 1.2pp.

3) *Surface*: Table VI shows that our single-frame model outperforms previous approaches. Loss weighting did not improve performance since the classes are fairly balanced. We could not use our multi-frame and sequential approaches since the task only allows for single-frame prediction. Our approach outperforms other approaches by a large margin. Table VII shows that a ResNet-18 backbone pre-trained for semantic segmentation on Vistas outperforms a ResNet-50 backbone pre-trained for classification on ImageNet-1k.

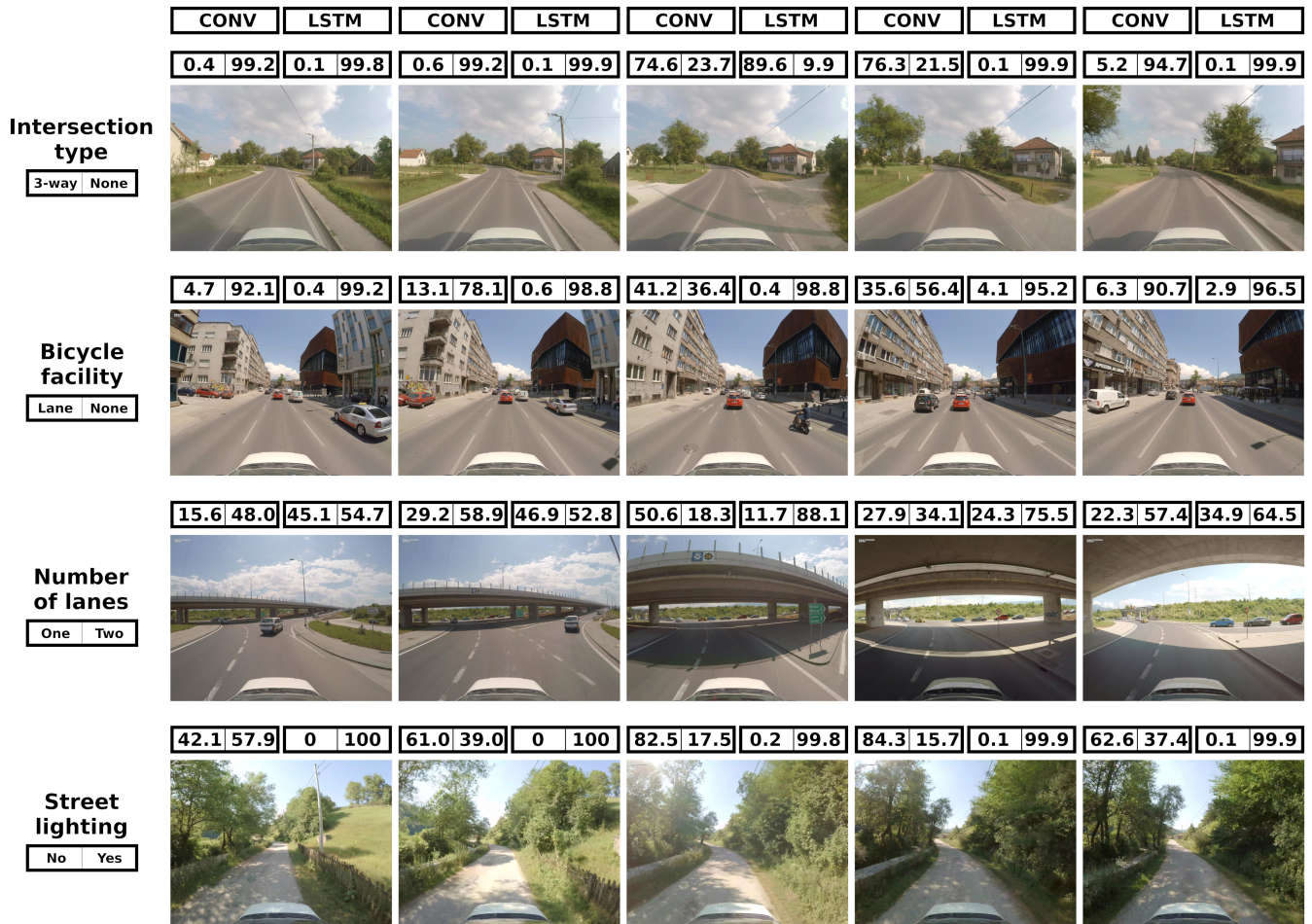


Fig. 3. Four examples in which sequential enhancement (LSTM) succeeds to correct visual predictions (conv). For each of the five consecutive segments (columns), we display categorical predictions by both models. Row 1 involves a single-peak attribute - *Intersection type*. We observe that the convolutional model incorrectly assigns a positive class (*3-way intersection*) in column 4. Rows 2 and 3 involve smooth attributes - *Bicycle facility* and *Number of lanes*. We observe that the convolutional model mistakes a motorcyclist near a tram rail for a dedicated bicycle lane in column 3 and fails to predict the correct number of lanes again in column 3. Row 4 involves the *Street lighting* attribute. We observe that the upcoming lighting poles are obscured by the road curvature and overgrown roadside bushes. Consequently, the convolutional model fails in columns 2-4. In all cases, the sequential model succeeds to correct the mistakes by leveraging a larger temporal context.

4) *Weather*: Table VIII shows that our single-frame model outperforms previous approaches on classes *Overcast*, *Snow*, and overall. It scored 2.23 pp and 1.95 pp lower than the best result on classes *Dry* and *Rain*, respectively. Similar to the Road Surface task, the classes in the Weather task are balanced, and loss weighting does not improve performance.

D. FM3m

We compare our method with the two of the best approaches provided by the authors of the FM3m dataset. They train SVM classifiers with RBF kernels on image descriptors obtained by ResNet-50 and DenseNet-121 networks pre-trained on ImageNet-1k. Table X shows that our single-frame model performs competitively. It should be noted that the networks which generated the image descriptors used in the two competing approaches were not fine-tuned on the FM3m dataset. After fine-tuning on the FM3 dataset, linear SVM classifiers trained on DenseNet-121 and ResNet-50 descriptors achieve mAP scores of 97.1% and 98.0%, respectively. We

also compare three different variants of our single-level model. Table XI shows that Vistas pre-training contributes more than using a larger backbone, such as ResNet-50.

VII. CONCLUSION

We have presented a two-stage approach for automatic recognition of road-safety attributes in monocular video. Our approach complements convolutional recognition with sequential enhancement and is able to detect more than forty road-safety attributes of the iRAP standard. Our multi-task convolutional model recovers a shared latent representation and subsequently processes it with per-attribute classification heads. The shared representation aggregates local features across several frames and benefits from pre-training on a large semantic segmentation dataset. We address the extreme class imbalance of iRAP attributes by proposing a multi-task variant of recall-based loss weighting. In this (multi-task) setup, the magnitudes of individual task losses are kept stable across batches to facilitate a comparable contribution

TABLE II
PER-ATTRIBUTE PERFORMANCE OF OUR BEST MODEL. M-F1 - MACRO-F1

Attribute	M-F1
Area type	94.56
Bicycle facility	100.00
Bicycle observed flow	34.83
Carriageway label	97.54
Curvature	64.77
Delineation	98.94
Grade	51.85
Intersection channelisation	62.74
Intersection quality	52.02
Intersection type	34.97
Land use - driver-side	63.85
Land use - passenger-side	69.60
Lane width	75.60
Median Type	55.62
Motorcycle observed flow	36.45
Number of lanes	98.49
Paved shoulder - driver-side	65.02
Paved shoulder - passenger-side	54.01
Pedestrian crossing - inspected road	45.03
Pedestrian crossing - side road	46.58
Pedestrian crossing quality	59.21
Pedestrian obs. flow across road	44.31
Pedestrian obs. flow along driver-side	29.37
Pedestrian obs. flow along passenger-side	35.62
Property access points	59.71
Quality of curve	71.24
Road condition	77.70
Roadside severity - driver-side distance	57.86
Roadside severity - driver-side object	43.31
Roadside severity - passenger-side distance	59.97
Roadside severity - passenger-side object	51.06
Roadworks	78.80
School zone crossing supervisor	66.51
School zone warning	68.03
Service road	62.26
Sidewalk - driver-side	43.72
Sidewalk - passenger-side	50.19
Sight distance	75.67
Skid resistance / grip	50.90
Speed management	100.00
Street lighting	91.53
Upgrade cost	63.28
Vehicle parking	60.28
Mean	62.86

to the total loss. A closer look at iRAP attributes reveals that different attribute types exhibit very different temporal behavior patterns. For instance, intersections occur at discrete moments in time, while the number of lanes remains constant through many frames. These considerations led us to enhance convolutional predictions with sequential post-processing. We

TABLE III
MACRO-F1 PERFORMANCE ON THE ROAD-PLACE TASK OF HONDA SCENES.

	BB	Road place	
		Mean	Mean w/o B
Honda BiLSTM [16]	RN50	27.56	25.23
Honda Event [16]	RN50	28.36	25.91
Context MTL [50]	RN50	-	27.92
Conv, CE (ours)	RN18	34.11	31.96
Conv, CE_{MT}^R (ours)	RN18	37.00	34.92
Conv+seq, CE_{MT}^R (ours)	RN18	40.93	39.00

design sequential enhancement as attribute-specific bidirectional recurrent models based on LSTM cells. The recurrent models learn to correct convolutional predictions by learning temporal behavior over a larger temporal context. The resulting predictions outperform the convolutional baseline across the board for all attributes.

We have experimentally demonstrated a substantial advantage of our contributions on three road-driving datasets: iRAP-BH, Honda Scenes, and FM3m. Our approach outperforms the previous work on all tasks of the Honda Scenes dataset. The greatest improvements occur on the Road place task due to sequential correction and alleviated class imbalance. Our approach also delivers competitive performance on the FM3m dataset in spite of a weaker backbone and the inability to leverage sequential post-processing.

We emphasize that our approach delivers competitive performance on a very low computational budget. Shared convolutional features are extracted by running an efficient ResNet-18 backbone once per frame. Per-attribute LSTM models operate on low-dimensional inputs, so training and inference are very fast. Preliminary experiments have shown that a straightforward causal adaptation can deliver road-safety assessments in real-time, even on a mobile device.

To summarize, our main contributions are semantic pre-training, multi-task recall-based loss weighting, and sequential enhancement. In addition, we introduce iRAP-BH as a novel dataset for visual road-safety assessment that specifically focuses on iRAP attributes. Future work should test the sensitivity of the proposed approach to various kinds of domain shift through evaluation on novel datasets. The new datasets should include multiple countries, different types of cameras, various seasons, and challenging meteorological conditions. Another promising research direction is to improve performance by leveraging dense prediction tasks such as panoptic segmentation and monocular reconstruction.

REFERENCES

- [1] World Health Organization, "Global status report on road safety 2018: Summary," 2018, WHO/NMH/NVI/18.20.
- [2] United Nations General Assembly, "Improving global road safety," 2020, A/RES/74/299.
- [3] L. Mooren, R. Grzebieta, and R. S. Job, "Safe system – comparisons of this approach in australia," in *Australasian College of Road Safety Conference "A Safe System: Making it Happen!"*, September 1-2, 2011, Melbourne, Australia, 2011.

TABLE IV

EXPERIMENTAL VALIDATION ON ALL SUBTASKS OF THE ROAD PLACE TASK OF HONDA SCENES. LEGEND: BB - BACKBONE; B-Background, I-Intersection, RC-Railway, C-Construction, LM-Left Merge, RM-Right Merge, LB-Left Branch, RB-Right Branch, OB-Overhead Bridge.

	BB	B	I5				RC				C				LM			RM		
			A	E	P	mean	A	E	P	mean	A	E	P	mean	A	P	mean	A	P	mean
Honda BiLSTM [16]	RN50	88	0	0	9	3	24	14	46	28	2	5	29	12	9	28	19	16	23	20
Honda Event [16]	RN50	92	0	0	0	0	23	47	46	39	2	6	38	15	5.6	8	7	13	16	15
Context MTL [50]	RN50	-	0	6	0	2	1	35	52	32	0	4	38	14	4	6	5	26	18	22
Conv, CE (ours)	RN18	90	19	0	5	8	13	49	52	38	2	11	56	23	22	29	26	29	33	31
Conv, CE _{MT} ^R (ours)	RN18	91	27	0	10	12	15	56	59	43	3	12	63	26	27	36	32	31	35	33
Conv+seq, CE _{MT} ^R (ours)	RN18	91	29	0	9	13	28	53	71	51	11	22	64	32	29	43	36	34	45	40
	BB	OB	I3				I4				LB			RB						
			A	E	P	mean	A	E	P	mean	A	P	mean	A	P	mean				
Honda BiLSTM [16]	RN50		23	55	53	44	3	28	27	19	14	68	66	49	36	22	29	28	28	28
Honda Event [16]	RN50		42	58	59	53	8	16	23	16	31	7	67	56	30	19	25	24	22	23
Context MTL [50]	RN50		47	59	60	55	11	38	28	26	14	78	79	57	33	19	26	34	27	31
Conv, CE (ours)	RN18		31	57	60	50	10	33	32	25	25	77	66	56	29	18	24	35	38	37
Conv, CE _{MT} ^R (ours)	RN18		33	58	61	51	10	34	34	26	26	77	68	57	31	23	27	37	42	40
Conv+seq, CE _{MT} ^R (ours)	RN18		37	59	64	53	14	32	38	28	30	78	73	60	42	24	33	41	44	43

TABLE V

MACRO-F1 PERFORMANCE ON THE ROAD ENVIRONMENT TASK OF HONDA SCENES.

	BB	Local	Highway	Ramp	Urban	mean
Honda Frame [16]	RN50	33	91	20	83	56.75
Context MTL [50]	RN50	36	92	21	81	57.5
Conv, CE _{MT} ^R (ours)	RN18	30.8	92.3	42.6	83.7	62.35
Conv+seq, CE _{MT} ^R (ours)	RN18	32.8	93.1	44.1	84.2	63.55

TABLE VI

MACRO-F1 PERFORMANCE ON THE ROAD SURFACE TASK OF HONDA SCENES.

	BB	Dry	Wet	Snow	mean	mean w/o Snow
Honda Frame [16]	RN50	93.00	92.00	99.70	94.90	92.50
Context MTL [50]	RN50	93.00	92.00	-	-	92.50
Conv single, CE _{MT} ^R (ours)	RN18	98.49	98.50	100.00	99.00	98.50

TABLE VII

ABLATION OF SEGMENTATION PRE-TRAINING (MACRO-F1) ON THE ROAD SURFACE TASK OF HONDA SCENES.

	BB	Dry	Wet	Snow	mean
IN-1k (ours)	RN18	97.17	96.81	99.67	97.88
IN-1k (ours)	RN50	97.67	97.32	99.67	98.22
Vistas (ours)	RN18	98.49	98.50	100.00	99.00

TABLE VIII

MACRO-F1 PERFORMANCE ON THE WEATHER TASK OF HONDA SCENES.

	BB	Clear	Overcast	Rain	Snow	mean	mean w/o Snow
Honda Frame [16]	RN50	92.00	83.00	96.00	94.00	91.25	90.33
Context MTL [50]	RN50	93.20	83.98	96.99	-	-	91.39
Conv single, CE _{MT} ^R (ours)	RN18	90.97	90.85	95.04	95.32	93.05	92.29

TABLE IX

ABLATION OF SEGMENTATION PRE-TRAINING (MACRO-F1) ON THE WEATHER TASK OF HONDA SCENES.

	BB	Clear	Overcast	Rain	Snow	mean
IN-1k (ours)	RN18	89.54	86.77	94.02	93.01	90.84
IN-1k (ours)	RN50	90.11	87.59	94.34	93.99	91.51
Vistas (ours)	RN18	90.97	90.85	95.04	95.32	93.05

TABLE X

AVERAGE PRECISION OF MULTI-LABEL CLASSIFICATION ON THE FM3M DATASET. LEGEND: H-Highway, R-Road, TU-Tunnel, E-Exit, S-Settlement, O-Overpass, B-Booth, TR-Traffic.

	H	R	Tu	E	S	O	B	Tr	mean
RN50-SVM [17]	99.84	91.13	99.94	97.70	98.33	97.15	98.75	86.75	96.20
DN121-SVM [17]	93.68	99.97	97.96	98.33	97.86	98.81	87.85	96.80	96.41
Conv single, CE _{MT} ^R (ours)	99.96	94.57	99.96	98.64	98.51	98.92	99.75	91.21	97.69

TABLE XI

ABLATION OF SEGMENTATION PRE-TRAINING (AP) ON THE FM3M DATASET. LEGEND: H-Highway, R-Road, TU-Tunnel, E-Exit, S-Settlement, O-Overpass, B-Booth, TR-Traffic.

	BB	H	R	Tu	E	S	O	B	Tr	mean
IN-1k (ours)	RN18	99.21	91.49	99.56	97.34	97.84	96.99	98.20	89.92	96.32
IN-1k (ours)	RN50	99.63	92.54	99.87	98.21	98.02	97.42	98.90	90.51	96.89
Vistas (ours)	RN18	99.96	94.57	99.96	98.64	98.51	98.92	99.75	91.21	97.69

- [4] B. F. Corben, D. B. Logan, L. Fanciulli, R. Farley, and I. Cameron, "Strengthening road safety strategy development 'towards zero' 2008–2020 – western australia's experience scientific research on road safety management swov workshop 16 and 17 november 2009," *Safety Science*, vol. 48, no. 9, pp. 1085–1097, 2010, scientific Research on Road Safety Management.
- [5] M. Green, C. Muir, J. Oxley, and A. Sobhani, "Safe system in road safety public policy: A case study from victoria, australia," *IATSS Research*, vol. 46, no. 2, pp. 171–180, 2022.
- [6] S. Aziz and S. Ram, "A meta-analysis of the methodologies practiced worldwide for the identification of road accident black spots," *Transportation Research Procedia*, vol. 62, pp. 790–797, 2022, 24th Euro Working Group on Transportation Meeting.
- [7] A. Adedokun, "Application of road infrastructure safety assessment methods at intersections," Ph.D. dissertation, Linköping University, 2016.
- [8] S. Job, "Advantages and disadvantages of reactive (black spot) and proactive (road rating) approaches to road safety engineering treatments: When should each be used?" in *Australasian Road Safety Research Policing Education Conference, 2012, Wellington, New Zealand, 2012*.
- [9] Road Safety Foundation, "Engineering Safer Roads: Star Rating roads for in-built safety," 2015.
- [10] iRAP - International Road Assessment Programme, "iRAP Star Rating and Investment Plan Implementation Support Guide," 2017.
- [11] Steve Lawson, "iRAP methodology and safer roadsides," 2017.
- [12] iRAP - International Road Assessment Programme, "iRAP Coding Manual Version 5.0 – Drive on Right Edition," 2019.
- [13] Y. Bengio, A. C. Courville, and P. Vincent, "Representation learning: A review and new perspectives," *IEEE Trans. Pattern Anal. Mach. Intell.*, vol. 35, no. 8, pp. 1798–1828, 2013.

- [14] G. Neuhold, T. Ollmann, S. R. Bulò, and P. Kotschieder, "The mapillary vistas dataset for semantic understanding of street scenes," in *IEEE International Conference on Computer Vision, ICCV 2017, Venice, Italy, October 22-29, 2017*. IEEE Computer Society, 2017, pp. 5000–5009.
- [15] J. Tian, N. C. Mithun, Z. Seymour, H. Chiu, and Z. Kira, "Striking the right balance: Recall loss for semantic segmentation," in *2022 International Conference on Robotics and Automation, ICRA 2022, Philadelphia, PA, USA, May 23-27, 2022*. IEEE, 2022, pp. 5063–5069.
- [16] A. Narayanan, I. Dwivedi, and B. Dariush, "Dynamic traffic scene classification with space-time coherence," in *International Conference on Robotics and Automation, ICRA 2019, Montreal, QC, Canada, May 20-24, 2019*. IEEE, 2019, pp. 5629–5635.
- [17] I. Sikiric, K. Brkic, P. Bevandic, I. Kreso, J. Krapac, and S. Segvic, "Traffic scene classification on a representation budget," *IEEE Trans. Intell. Transp. Syst.*, vol. 21, no. 1, pp. 336–345, 2020.
- [18] S. Chatterjee and S. Mitra, "Safety assessment of two-lane highway using a combined proactive and reactive approach: Case study from indian national highways," *Transportation Research Record*, vol. 2673, no. 7, pp. 709–721, 2019.
- [19] H. Cui, J. Dong, M. Zhu, X. Li, and Q. Wang, "Identifying accident black spots based on the accident spacing distribution," *Journal of Traffic and Transportation Engineering (English Edition)*, 2022.
- [20] B. Dimitrijevic, S. Darban Khaless, R. Asadi, and J. Lee, "Short-term segment-level crash risk prediction using advanced data modeling with proactive and reactive crash data," *Applied Sciences*, vol. 12, p. 856, 01 2022.
- [21] S. M. Gaweesh, M. M. Ahmed, and A. V. Piccorelli, "Developing crash prediction models using parametric and nonparametric approaches for rural mountainous freeways: A case study on wyoming interstate 80," *Accident Analysis & Prevention*, vol. 123, pp. 176–189, 2019.
- [22] H. Stipdonk, S. Job, and B. Turner, "The safe system approach in action," *ITF*, 2022.
- [23] S. He, M. A. Sadeghi, S. Chawla, M. Alizadeh, H. Balakrishnan, and S. Madden, "Inferring high-resolution traffic accident risk maps based on satellite imagery and GPS trajectories," in *2021 IEEE/CVF International Conference on Computer Vision, ICCV 2021, Montreal, QC, Canada, October 10-17, 2021*. IEEE, 2021, pp. 11957–11965.
- [24] D. Tabernik and D. Skocaj, "Deep learning for large-scale traffic-sign detection and recognition," *IEEE Trans. Intell. Transp. Syst.*, vol. 21, no. 4, pp. 1427–1440, 2020.
- [25] S. Segvic, K. Brkic, Z. Kalafatic, and A. Pinz, "Exploiting temporal and spatial constraints in traffic sign detection from a moving vehicle," *Mach. Vis. Appl.*, vol. 25, no. 3, pp. 649–665, 2014.
- [26] Q. Zou, H. Jiang, Q. Dai, Y. Yue, L. Chen, and Q. Wang, "Robust lane detection from continuous driving scenes using deep neural networks," *IEEE Trans. Veh. Technol.*, vol. 69, no. 1, pp. 41–54, 2020.
- [27] V. Zadrija, J. Krapac, S. Segvic, and J. Verbeek, "Sparse weakly supervised models for object localization in road environment," *Comput. Vis. Image Underst.*, vol. 176-177, pp. 9–21, 2018.
- [28] J. C. McCall and M. M. Trivedi, "Video-based lane estimation and tracking for driver assistance: survey, system, and evaluation," *IEEE Trans. Intell. Transp. Syst.*, vol. 7, no. 1, pp. 20–37, 2006.
- [29] S. R. Bulò, L. Porzi, and P. Kotschieder, "In-place activated batchnorm for memory-optimized training of dnn," in *2018 IEEE Conference on Computer Vision and Pattern Recognition, CVPR 2018, Salt Lake City, UT, USA, June 18-22, 2018*. Computer Vision Foundation / IEEE Computer Society, 2018, pp. 5639–5647.
- [30] B. Cheng, A. G. Schwing, and A. Kirillov, "Per-pixel classification is not all you need for semantic segmentation," in *Advances in Neural Information Processing Systems 34: Annual Conference on Neural Information Processing Systems 2021, NeurIPS 2021, December 6-14, 2021, virtual*, M. Ranzato, A. Beygelzimer, Y. N. Dauphin, P. Liang, and J. W. Vaughan, Eds., 2021, pp. 17864–17875.
- [31] I. Krešo, J. Krapac, and S. Segvic, "Efficient ladder-style densenets for semantic segmentation of large images," *IEEE Trans. Intell. Transp. Syst.*, pp. 1–11, 2020.
- [32] M. Orsic, I. Kreso, P. Bevandic, and S. Segvic, "In defense of pre-trained imagenet architectures for real-time semantic segmentation of road-driving images," in *Proc. CVPR*. Computer Vision Foundation / IEEE, 2019, pp. 12607–12616.
- [33] T. G. P. Sanjeevani and B. K. Verma, "Learning and analysis of ausrap attributes from digital video recording for road safety," in *Proc. IVCNZ*. IEEE, 2019, pp. 1–6.
- [34] Z. Jan, B. Verma, J. Affum, S. Atabak, and L. Moir, "A convolutional neural network based deep learning technique for identifying road attributes," in *2018 International Conference on Image and Vision Computing New Zealand (IVCNZ)*, 2018, pp. 1–6.
- [35] P. Sanjeevani and B. Verma, "An optimisation technique for the detection of safety attributes using roadside video data," in *2020 35th International Conference on Image and Vision Computing New Zealand (IVCNZ)*, 2020, pp. 1–6.
- [36] H. Yi, C. Bizon, D. Borland, M. Watson, M. Satusky, R. Rittmuller, R. Radwan, R. Srinivasan, and A. Krishnamurthy, "Ai tool with active learning for detection of rural roadside safety features," in *2021 IEEE International Conference on Big Data (Big Data)*, 2021, pp. 5317–5326.
- [37] M. Kacan, M. Orsic, S. Segvic, and M. Sevrovic, "Multi-task learning for irap attribute classification and road safety assessment," in *23rd IEEE International Conference on Intelligent Transportation Systems, ITSC 2020, Rhodes, Greece, September 20-23, 2020*. IEEE, 2020, pp. 1–6.
- [38] A. Fernández, S. García, M. Galar, R. C. Prati, B. Krawczyk, and F. Herrera, *Learning from Imbalanced Data Sets*. Springer, 2018.
- [39] P. Bevandic, M. Oršic, I. Grubišic, J. Šaric, and S. Šegvic, "Multidomain semantic segmentation on datasets with overlapping classes," *arXiv preprint arXiv:2009.01636*, 2021.
- [40] I. Kreso, D. Causevic, J. Krapac, and S. Segvic, "Convolutional scale invariance for semantic segmentation," in *Proc. GCPR*, B. Rosenhahn and B. Andres, Eds., 2016.
- [41] C. Huang, Y. Li, C. C. Loy, and X. Tang, "Learning deep representation for imbalanced classification," in *2016 IEEE Conference on Computer Vision and Pattern Recognition, CVPR 2016, Las Vegas, NV, USA, June 27-30, 2016*. IEEE Computer Society, 2016, pp. 5375–5384.
- [42] Y. Wang, D. Ramanan, and M. Hebert, "Learning to model the tail," in *Advances in Neural Information Processing Systems 30: Annual Conference on Neural Information Processing Systems 2017, December 4-9, 2017, Long Beach, CA, USA*, I. Guyon, U. von Luxburg, S. Bengio, H. M. Wallach, R. Fergus, S. V. N. Vishwanathan, and R. Garnett, Eds., 2017, pp. 7029–7039.
- [43] Y. Cui, M. Jia, T. Lin, Y. Song, and S. J. Belongie, "Class-balanced loss based on effective number of samples," *CoRR*, vol. abs/1901.05555, 2019.
- [44] S. Hochreiter and J. Schmidhuber, "Long short-term memory," *Neural Comput.*, vol. 9, no. 8, pp. 1735–1780, 1997.
- [45] J. Y. Ng, M. J. Hausknecht, S. Vijayanarasimhan, O. Vinyals, R. Monga, and G. Toderici, "Beyond short snippets: Deep networks for video classification," in *IEEE Conference on Computer Vision and Pattern Recognition, CVPR 2015, Boston, MA, USA, June 7-12, 2015*. IEEE Computer Society, 2015, pp. 4694–4702.
- [46] H. Xu, A. Das, and K. Saenko, "R-C3D: region convolutional 3d network for temporal activity detection," in *IEEE International Conference on Computer Vision, ICCV 2017, Venice, Italy, October 22-29, 2017*. IEEE Computer Society, 2017, pp. 5794–5803.
- [47] Y. Chao, S. Vijayanarasimhan, B. Seybold, D. A. Ross, J. Deng, and R. Sukthankar, "Rethinking the faster R-CNN architecture for temporal action localization," in *2018 IEEE Conference on Computer Vision and Pattern Recognition, CVPR 2018, Salt Lake City, UT, USA, June 18-22, 2018*. Computer Vision Foundation / IEEE Computer Society, 2018, pp. 1130–1139.
- [48] Y. Tu, J. Du, L. Sun, and C. Lee, "Lstm-based iterative mask estimation and post-processing for multi-channel speech enhancement," in *2017 Asia-Pacific Signal and Information Processing Association Annual Summit and Conference, APSIPA ASC 2017, Kuala Lumpur, Malaysia, December 12-15, 2017*. IEEE, 2017, pp. 488–491.
- [49] F. Kratzert, D. Klotz, C. Brenner, K. Schulz, and M. Herrnegger, "Rainfall-runoff modelling using long short-term memory (lstm) networks," *Hydrology and Earth System Sciences*, vol. 22, no. 11, pp. 6005–6022, 2018.
- [50] Y. Lee, J. Jeon, J. Yu, and M. Jeon, "Context-aware multi-task learning for traffic scene recognition in autonomous vehicles," in *IEEE Intelligent Vehicles Symposium, IV 2020, Las Vegas, NV, USA, October 19 - November 13, 2020*. IEEE, 2020, pp. 723–730.
- [51] R. D. Hjelm, A. Fedorov, S. Lavoie-Marchildon, K. Grewal, P. Bachman, A. Trischler, and Y. Bengio, "Learning deep representations by mutual information estimation and maximization," in *7th International Conference on Learning Representations, ICLR 2019, New Orleans, LA, USA, May 6-9, 2019*. OpenReview.net, 2019.
- [52] K. He, X. Zhang, S. Ren, and J. Sun, "Spatial pyramid pooling in deep convolutional networks for visual recognition," *IEEE Trans. Pattern Anal. Mach. Intell.*, vol. 37, no. 9, pp. 1904–1916, 2015.
- [53] Ö. Yildirim, "A novel wavelet sequence based on deep bidirectional LSTM network model for ECG signal classification," *Comput. Biol. Medicine*, vol. 96, pp. 189–202, 2018.
- [54] Z. C. Lipton, C. Elkan, and B. Narayanaswamy, "Optimal thresholding of classifiers to maximize F1 measure," in *Machine Learning and Knowledge Discovery in Databases - European Conference, ECML*

PKDD 2014, Nancy, France, September 15-19, 2014. Proceedings, Part II, ser. Lecture Notes in Computer Science, T. Calders, F. Esposito, E. Hüllermeier, and R. Meo, Eds., vol. 8725. Springer, 2014, pp. 225–239.

- [55] J. Opitz and S. Burst, “Macro F1 and macro F1,” *CoRR*, vol. abs/1911.03347, 2019.

VIII. BIOGRAPHY SECTION



Marin Kačan received his MSc degree in computer science the University of Zagreb. He spent two years as an expert associate at the Faculty of Traffic and Transport Sciences, University of Zagreb. Currently he is a young researcher and a PhD student at the Faculty of Electrical Engineering and Computing, University of Zagreb. His research addresses image and video classification with a focus on road infrastructure assessment.



Marko Ševrović is a senior road safety engineer with more than 15 years of experience in the field of traffic flow theory, public transport planning, transport infrastructure design and road safety. He holds a PhD degree in the field of traffic and transport technology from Faculty of Transport and Traffic Sciences, University of Zagreb, Croatia, where he works part-time as an Associate Professor and Head of Department of Transport Planning. In September 2018 he became part-time employee of the European Institute of Road Assessment (EuroRAP).

He conducted and participated in more than 200 national and international professional and scientific projects in the field of road safety (EuroRAP/iRAP projects, Road Safety Audit), traffic planning and sustainable urban mobility planning. He is a chartered engineer and road safety auditor.



Siniša Šegvić received his Ph.D. degree in computer science from the University of Zagreb, Croatia. He was a post-doctoral Researcher at IRISA Rennes and TU Graz. He is currently a Full Professor at the Faculty of Electrical Engineering and Computing, University of Zagreb. His research interests include computer vision and deep learning, with special interests in natural scene understanding for autonomous vehicles and safe traffic.